Pantoja, M. et al. Development of superhydrophobic coatings on AISI 304 austenitic stainless steel with different surface pretreatments, in: *Thin solid films, Vol. 671, Feb. 2019, Pp. 22-30*

DOI: https://doi.org/10.1016/j.tsf.2018.12.016

Development of superhydrophobic coatings on AISI 304 austenitic stainless steel with different surface pretreatments

M. Pantoja*, F. Velasco, J. Abenojar, M.A. Martinez

Department of Materials Science and Engineering, IAAB, Universidad Carlos III de Madrid, Av Universidad 30, 28911 Leganés, Spain

ARTICLE INFO

Keywords:
Pretreatment
Superhydrophobic coating
Stainless steel

ABSTRACT

In the context of increasing industrial importance of superhydrophobic surfaces, three different pretreatments on an austenitic stainless steel surface have been tested to be coated with a silane-based solution containing SiO_2 nanoparticles, in order to obtain superhydrophobic surfaces. The pretreatments are (i) an acetone degreaser, (ii) this one followed by a hot air treatment and acid pickling, and (iii) the previous one followed by an alkaline etching. Pretreated surfaces have been characterized by X-ray photoelectron spectroscopy, tapping-mode atomic force microscopy and contact angle measurements. After the three pretreatments, a solution of methyltrimethoxysilane and tetraethoxysilane in white spirit solvent and 1% of SiO_2 (% by wt.) has been used to prepare a superhydrophobic coating on them. The hydrophobicity of the developed coatings has been studied using water contact angle measurements (static angles and advancing and receding angles). Besides, scanning electron microscope has been used to study the coatings. The results show that different tailored surfaces can be obtained in stainless steels using these pretreatments, obtaining surfaces that exhibit different physicochemical characteristics that may condition the formation of superhydrophobic coatings on them.

1. Introduction

Nature has been the inspiration source to artificially develop superhydrophobic surfaces. Numerous examples of natural superhydrophobic surfaces [1] have been used for a better understanding about this phenomenon. During last years, research on superhydrophobic surfaces has been widely developed due to their numerous industrial applications [2]. Different researchers show that it is possible to artificially generate hydrophobic surfaces by reproducing the surface patterns observed in nature, using different techniques (lithography, templating, plasma treatment, sol-gel methods) [1,3]. However, some of these methods alter the aesthetic appearance of the substrate. Different studies show that sol-gel methods are an adequate alternative to create superhydrophobic, transparent coatings.

Such sol-gel coatings are based on the use of SiO_2 nanoparticles and silanes in a solvent. Either by dip coating or by spraying, robust, transparent and superhydrophobic coatings have been prepared on glass [4–10]. The approaches mainly vary in the solvent, the specific selected silane and the coating procedure. Other authors have demonstrated the ability of the same method to manufacture superhydrophobic coatings on metals (germanium, brass, steel, copper) [11], wood [12] or polyester mesh [13].

The achievement of superhydrophobic surfaces on stainless steel has been mainly done by electrodeposition of hydrophobic polymers [14], thermal plasma evaporation methods [15], or laser [16–18], but sol-gel methods have also been studied [19–22]. However, no information about pretreatment of stainless steel is given, and the effect of pretreatment on coating formation has not been analyzed as in this work. Pretreatments on stainless steels are generally used for changing their aesthetical aspect or enhancing their durability. It is clear that those pretreatments can affect the formation of hydrophobic coatings on them, as they can change their surface composition, as occur with treatments up to 300 °C [23] or scales [24].

Milionis et al. [2] underlined that the most important aspect that can further improve the adhesion of superhydrophobic coatings is the appropriated physical and chemical modification of the substrates before the application of a coating. This research tries to achieve a deeper understanding of the superhydrophobicity phenomenon [2], evaluating the influence of the pretreatment to modify the surface and hence to achieve a superhydrophobic coating. In order to attain this aim, a well-known solution to get hydrophobicity [25], based on a mix of silanes and SiO_2 nanoparticles, has been employed to coat stainless steel substrates with different pretreatments before the application of the superhydrophobic coating.

* Corresponding author.
E-mail address: mpruiz@ing.uc3m.es (M. Pantoja).

2. Experimental procedure

2.1. Materials and pretreatments

Tetraethoxysilane ($Si(OCH_2CH_3)_4$, TEOS) and methyltrimethoxysilane ($CH_3Si(OCH_3)_3$, MTS) were supplied by ABCR GmbH & Co. KG (Karlsruhe, Germany). White spirit (WS) was used as solvent. It is a commercial product, containing less than 0.1% wt. benzene. Fumed silica powder, surface-treated with polydimethylsiloxane (AEROSIL® R202), was supplied by Evonik Industries (Essen, Germany), with a particle size of 14 nm.

The substrate used to deposit the coating onto was a burnished AISI 304 austenitic stainless steel. It was supplied with three different surface pretreatments. The easiest one was a degrease cleaning with acetone (pretreatment labelled as A_0). Moreover, the stainless steel suffered two different pretreatments, one based on acid pickling (labelled as A_1), and another of an alkaline etching after previous acid pickling (A_2). A_1 surface was manufactured in two steps. The stainless steel was exposed to a dynamic air flow (at 200 °C for 5 h) and then it was immersed in a phosphoric acid solution (Ferrophos 7773®, Alufinish) at 55 °C for 2 min, rinsed with water and dried. A_2 surface was made immersing A_1 samples in an alkaline solution (TURCO 4215-S®, Henkel) at 60 °C for 15 min, and then rinsed with plenty water and dried. The three pretreatments were developed to achieve physically and chemically different surfaces and hence to study the ability to develop superhydrophobic coatings using a sol-gel process. Table 1 summarizes the studied surfaces that show no significant differences in measured R_a (macroroughness) values.

2.2. Preparation of sol-gel solutions and superhydrophobic coatings

Sol-gel solution was prepared as described in previous research [25] using WS as solvent. Nanometric SiO_2 was added (1% by wt.) to the solution and this mixture was stirred for 15 min before applying the superhydrophobic coating. As previously reported [25], the size of SiO_2 agglomerates in this silane-WS solution is small, around 25–43 nm.

Superhydrophobic coatings were applied by dip coating using a Zr 4200 Dip Coater (Delta Instruments, JB Drachten, Netherlands), as described previously [25]. The withdrawal speed was 400 mm/min and the immersion time in the solution was 1 min. Coatings were prepared with one or three immersions in the solutions. The standby time between immersions was 3 min.

2.3. Characterization of surfaces

The chemical composition of the stainless steels with the three considered surface conditions was investigated by X-ray photoelectron spectroscopy (XPS) analysis with a VG Scientific Microtech Multilab (VG Scientific, Hastings, UK) equipment, using a Mg-K_α (1253.6 eV) X-ray source (SPECS XR-50) operating at 15 keV and 300 W. Residual pressure was kept below $5{\cdot}10^{-8}$ Torr. A survey scan was carried out within the 0–1200 eV region. High resolution spectra were then performed at 20 eV pass energy. All binding energies were referred to the C (1 s) core level spectrum position for C–C species at 285 eV, subtracting a Shirley background. Curve fittings were performed using Gaussian-Lorentzian fits. Atomic concentrations were calculated using VGX900-W XPS-surface analysis software.

Contact angle was measured on stainless steels using an OCA 15 plus goniometer from DataPhysics (Neurtek Instruments, Eibar, Spain). Five test liquids (deionised water, glycerol, ethylenglycol, 1.5-pentanediol and diidomethane), covering a wide range of surface tensions and polarities, were chosen to calculate the surface energy of the different surfaces. Drops (3 µl) of liquid were deposited on surfaces using a micrometric syringe. Contact angles were measured five times with each liquid in different locations and the mean value was computed. All components of surface energy were obtained by means of the Owens-Wendt-Rable-Kaelble (OWRK) method.

In order to study a possible relationship between pretreatment affects and the wetting ability of this solution on pretreated surfaces, surface tension of silane-based solution was evaluated by pendant drop method. Moreover, the contact angle of the solution on pretreated surfaces was evaluated by sessile drop method.

Pretreatment effects on the topography of the stainless steel were investigated by tapping-mode atomic force microscopy (AFM). The AFM measurements were carried out in air using MultiMode NanoScope IV equipment (Digital Instruments, Veeco Metrology Group, Santa Barbara, USA), employing silicon tips with a constant force of about 40 N/m and a resonance frequency close to 300 kHz. Nanoroughness was measured on flattened images.

Superhydrophobic coatings were studied by water contact angle measurements, in the same previously indicated conditions, and by scanning electron microscope (SEM). The SEM study was carried out using FEI TENEO equipment (Eindhoven, Netherlands) coupled with an energy dispersive X-ray spectrometry (EDS) semiquantitative analyzer. The samples were analyzed without sputtering.

The method used to evaluate the mechanical robustness of these coatings was a linear abrasion test, as previously described in other researches [26,27]. Scratch equipment (Elcometer 3000, Manchester, UK) with a cylindrical abrasive head (8 mm of diameter) was used, applying on the coated surface a normal load (200 g) at constant speed (30 mm/s) and using a P2500 SiC sandpaper as abrasive. All tests were carried out at room temperature (22 °C) and 30% relative humidity for one and two abrasion cycles. After each abrasion test, water contact angles were measured on the tested surface to evaluate its hydrophobicity. Besides, the morphology of worn coatings was analyzed by SEM.

3. Results and discussion

3.1. Characterization of stainless steel surfaces

The global XPS surveys of the three pretreated surfaces are shown in Fig. 1 (left). The XPS spectra reveal that the passive layer generated on pretreated stainless steels comprises primarily iron and chromium. The following peaks appeared for all surfaces and they are assigned to: 2p signal of Fe (from 705 to 720 eV), 2p signal of Cr (from 572 to 594 eV), 1 s signal of O (from 525 to 540 eV) and 1 s signal of C (from 282 to 290 eV) [28–30]. The corresponding binding energies of these deconvoluted peaks, which agree with literature [31–33], are summarized in Table 2. Carbon signal is due to contamination, being usual in XPS spectra. This peak decreases when A_1 and A_2 pretreatments are applied.

Differences can be appreciated qualitatively among all spectra, indicating that different chemistries were attained in surfaces, as required to evaluate the influence of pretreatment on the formation of

Table 1
Summary of pretreatments and the achieved roughness (R_a).

Substrate	Studied surface	Pretreatment	R_a (µm)
Austenitic stainless steel	A_0	Acetone degreaser	0.27 ± 0.02
	A_1	A_0 + Hot air treatment + Acid pickling	0.25 ± 0.02
	A_2	A_1 + alkaline etching	0.25 ± 0.03

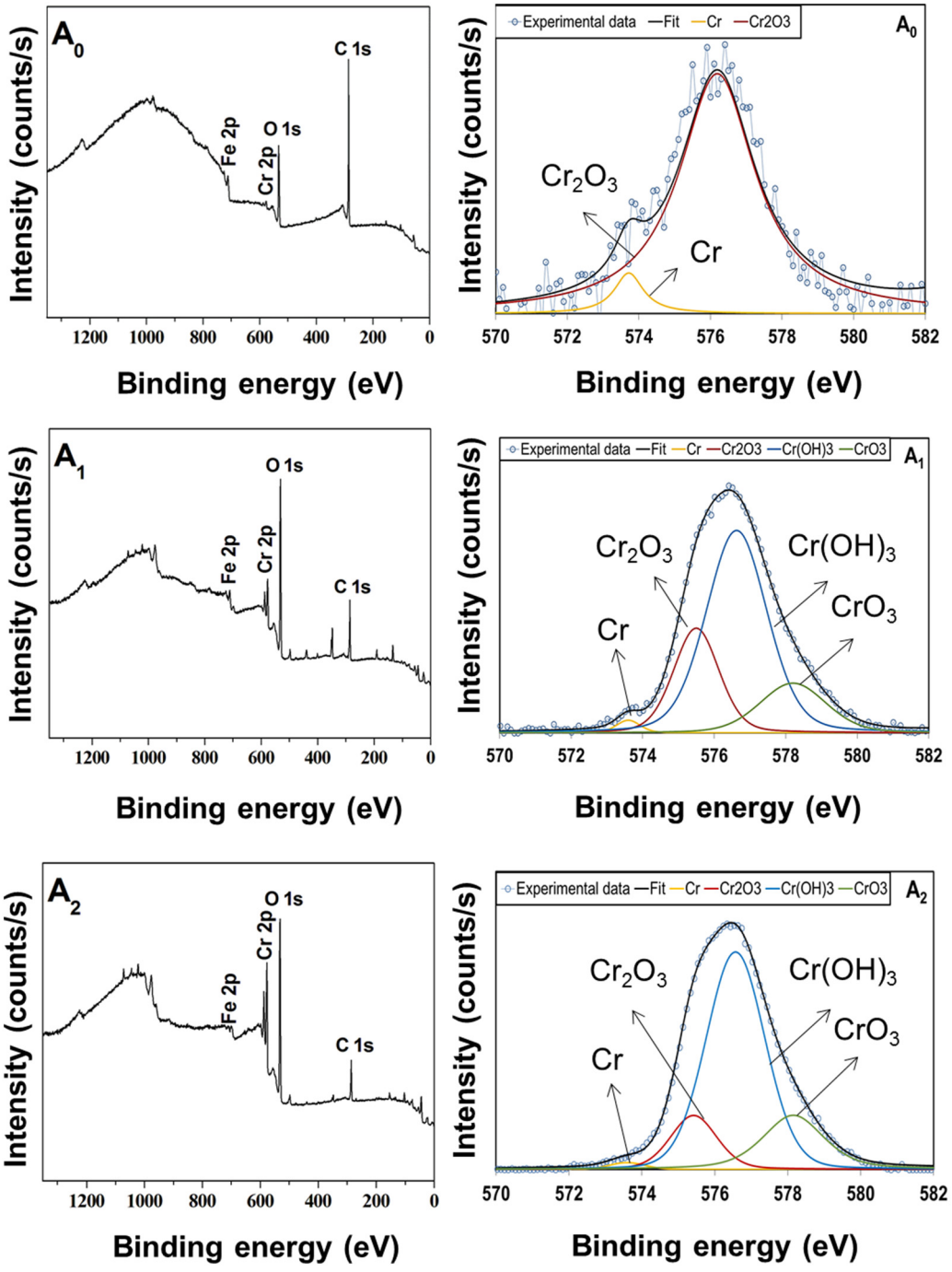

Fig. 1. XPS of pretreated stainless steels. Left, complete survey. Right, Cr 2p3/2 core levels spectra.

Table 2
Cr 2p3/2 and 2p1/2 deconvoluted peak position from XPS signals.

Specie	Binding energy (eV)					
	A_0		A_1		A_2	
	$2p_{3/2}$	$2p_{1/2}$	$2p_{3/2}$	$2p_{1/2}$	$2p_{3/2}$	$2p_{1/2}$
Cr	573.72	583.6	573.60	583.61	573.60	583.53
Cr_2O_3	576.19	586.1	575.50	585.11	575.40	585.23
$Cr(OH)_3$	–	–	576.63	586.61	576.57	586.43
Cr^{6+}	–	–	578.20	588.61	578.15	588.03

superhydrophobic coatings. These differences can be clearly appreciated, for instance, in Cr peak, where different species are present in each pretreated surface, as the deconvolutions of the Cr_{2p} high resolution spectra show (Fig. 1 right). The Cr_{2p} peak corresponding to A_0 was deconvoluted using Gaussian-Lorenztian fitting into two peaks (assigned to Cr and Cr_2O_3). For A_1 and A_2, good fit is provided when these peaks are deconvoluted into four components (assigned to Cr, Cr_2O_3, $Cr(OH)_3$ and Cr^{6+}). In all three cases, $Cr_{2p3/2}$ and $Cr_{2p1/2}$ components have the expected 2:1 ratio and an energy difference of 9.8 eV approximately (Table 2).

Fig. 2 shows the elemental composition of the surface layer of different pretreated stainless steels. Me^{n+}/Me ratio calculated from XPS analysis (Fig. 2, being Me the addition of iron and chromium in metallic state and Me^{n+} the addition of their cations) informs that the thickness

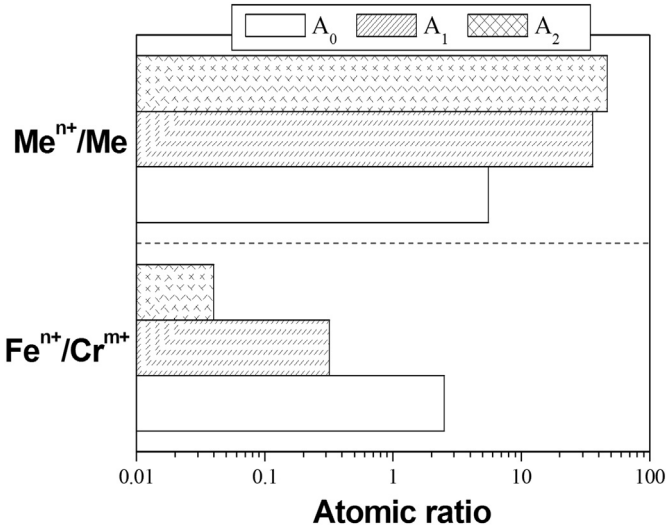

Fig. 2. Elemental composition of the surface layer as function of pretreatment by XPS.

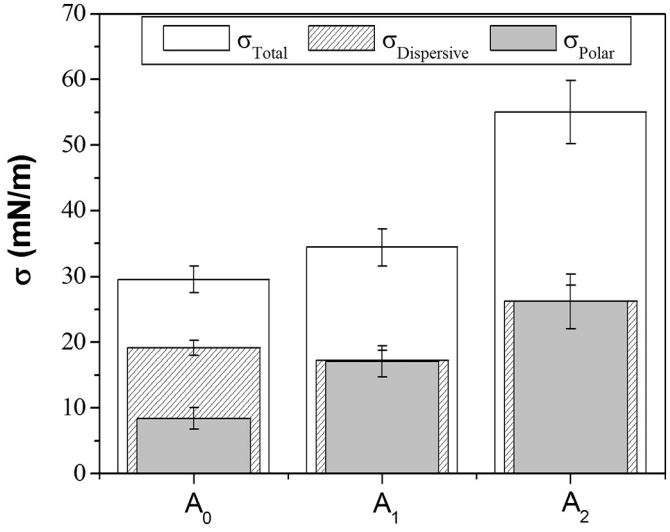

Fig. 4. Surface energy of pretreated stainless steels and its dispersive and polar components.

of oxide film depends on the pretreatment. A_2 and A_1 surfaces show an oxide film thicker than A_0, being both metallic Fe and metallic Cr (as shown for the latter in Fig. 1 right) found in XPS spectra. The compositional characteristics of the oxide layer are evaluated from the ratio of Fe ions to Cr ions (Fig. 2). A_0 surface is richer in iron than in chromium species, while A_1 and A_2 surfaces show higher amount of chromium species, being A_2 surface the richest. This chromium enrichment of the surface oxide layer for stainless steel in its passive state has been well-documented previously [34]. Acid pickling of the surface has provoked the removal of iron species, that are easily removable under these conditions, provoking that the passive layer is strongly Cr-rich. Further alkaline etching increases iron species removal.

Apart from Cr signal from base metal, the relative amount of chromium species in the surface layer for the different surfaces is shown in Fig. 3. The effect of surface pretreatments on the chemistry of the surface is clear. A_0 pretreated surface only comprises Cr_2O_3. This could be expected as no specific pretreatment to change its chemistry was carried out. In this case, passive stainless steel usually shows an internal Cr_2O_3 layer with Fe oxides outside (as Fe^{n+}/Cr^{m+} values in Fig. 2 show). Cr^{6+} and $Cr(OH)_3$ species are only observed on the surface layer after A_1 and A_2 pretreatments, being $Cr(OH)_3$ the predominant specie observed on both surfaces. No meaningful differences in Cr species are attained between A_1 and A_2 pretreatments, underlying that alkaline

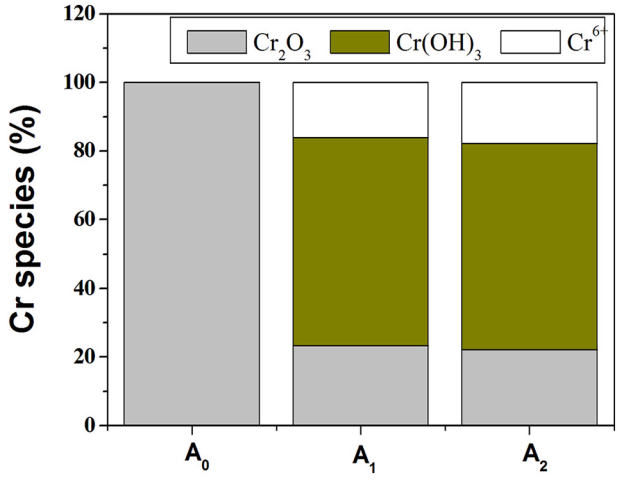

Fig. 3. Cr species in the passive layer from Cr deconvoluted signal.

etching after acid pickling mainly affects iron species (Fig. 2). The presence of Cr^{6+} species on stainless steel surface, after pretreatment with an acid solution, has been previously reported by Brooks et al. [35]. High content of $Cr(OH)_3$ species has been reported by Hermas et al. [31] on the oxide film of an austenitic stainless steel coated with conductive polymer when it was exposed to an acid solution. The iron dissolution from the passive layer has been previously shown [34] when combining acid and alkaline treatments, confirming Cr enrichment as shown in Fig. 2.

Surface energy and its polar and dispersive components are shown in Fig. 4 for the different pretreated surfaces (A_0, A_1 and A_2). Surface energy values lower than 35 mN/m are measured for A_0, being the dispersive component fraction higher than the polar one. Similar values of surface energy were found by Mantel et al. [36] on solvent-cleaned 304 stainless steel. A_1 shows slightly higher surface energy values, while surface energy increases to around 55 mN/m for A_2. In both cases, there is a marked increase of the polar component, being equal both dispersive and polar components.

These results show that increased values of polar component are observed for the Cr-rich surfaces (A_1 and A_2). Two effects provoke this change in surface energy and polarity. On one hand, cleaning of the surface has taken place, removing carbon moieties, as it can be seen qualitatively in Fig. 1 (left) for A_1 and A_2 pretreatments. Different researches [34,36] observe a significant increase of the polar component for pretreated stainless steel and they suggest that the increase of the polar fraction is related to a reduction of surface contamination. When the surface is cleaned with organic solvents, carbonaceous residuals can be left on the surface, while other pretreatments (as polishing, thermal oxidation or plasma) reduce the surface contamination more efficiently [34,36]. This should explain the low wettability and high dispersive component measured for A_0. On the other hand, the chemical effects taking place during A_1 and A_2 pretreatments are so important that cannot be discarded to explain the increase of surface energy. Fe has almost disappeared from the surface layer (Fig. 2) and Cr species are responsible for the increase of the polar component of surface energy. The presence of Cr hydroxide on the surface is dominant, and its polar OH^- groups can strongly affect the polarity of the surface after A_1 and A_2 pretreatments. This effect has also been demonstrated for other Cr surfaces [37], indicating that the amount of hydroxide on the surface plays a major role on surface wettability.

A_1 and A_2 pretreatments do not show dramatic chemical differences able to explain the changes in surface energy between them. Padial-Molina et al. [38] pretreated silicon surfaces using alkaline solution and

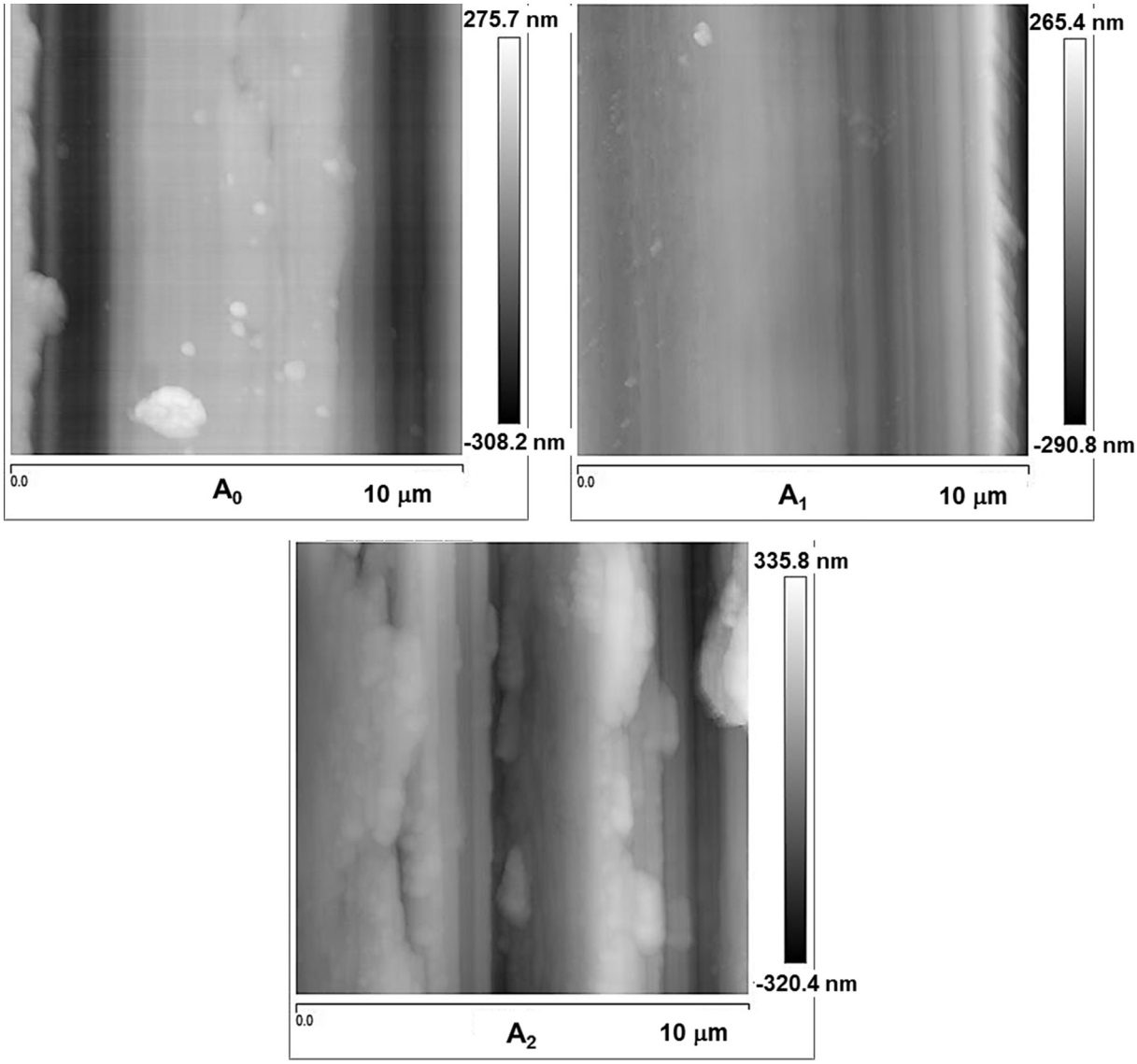

Fig. 5. AFM images (3D-view) of pretreated surfaces, at two different magnifications.

observed topography changes with the immersion time in the solution and a relationship between nanoroughness and wettability. The nanoroughness increased with immersion time in alkaline solution and higher water contact angle values were measured. So, nanoroughness differences between A_1 and A_2 could explain the improvement of wettability observed for A_2.

Surface tension of silane-based solution (22 ± 1 mN/m) was measured using pendant drop method. This value is lower than the surface energy of all pretreated surfaces (Fig. 4), meaning that this solution can wet the three surfaces. This was checked measuring the contact angle of this solution on each pretreated steel. Contact angles lower than 10° were measured for all surfaces.

AFM study (Fig. 5) shows a morphological analysis of the three surfaces to evaluate the pretreatment effects on the nanoscale. Fig. 5 (left) shows the images at smaller magnification than Fig. 5 (right). It can be seen how the nanoroughness increases with chemical pretreatments (A_1 and A_2), changing dramatically the material topography. It is clear that the used pretreatments have changed the topography, confirming that acid pickling has removed the outer part of the passive layer comprising iron species, promoting a textured surface which increases the nanoroughness (Table 3). It has to be pointed out that these changes in topography take place at nanolevel, but not at micro level, being not found roughness differences among these surfaces, as values around 25 µm are measured after the three pretreatments (Table 1). Hence pretreatments change both physically and chemically the surface, supporting the idea that carbon moieties reduction is not the only effect to explain surface energy results.

Table 3
Nanoroughness values from AFM images for the three considered pretreatments.

	A_0	A_1	A_2
R_a (nm)	2.1 ± 0.3	6.1 ± 0.5	4.5 ± 0.8

Table 3 summarizes nanoroughness measurements. The smooth topography of the A_0 surface (Fig. 5) leads to lowest roughness values. It is noticeable that A_1 and A_2 pretreatments show slightly higher roughness values. This agrees with the removal provoked by acid and/or alkaline solutions. The effect seems to be slightly more marked for A_1 surface.

So different tailored surfaces can be obtained in stainless steels, with different physicochemical characteristics, that may influence the formation of superhydrophobic coatings.

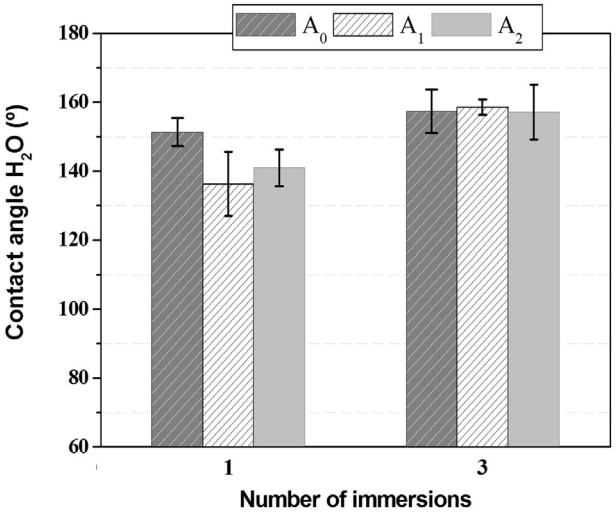

Fig. 6. Static water contact angles on coated surfaces after one and three immersions.

3.2. Characterization of coatings

Static water contact angle measurements were carried out to study the hydrophobic behavior of the coated surfaces. Results are shown in Fig. 6. Water contact angles higher than 150° are measured for all coatings prepared after three immersions. For one immersion, the only coating displaying contact angles over 150° is the deposited coating on A_0 surface. Average contact angles around 137° and 142° are measured for coatings prepared on A_1 and A_2 after one immersion, respectively. These water contact angles are meaningfully higher than the angles measured on the pretreated surfaces (Fig. 8, uncoated steel), being 98 ± 9°, 62 ± 4° and 51 ± 6° for A_0, A_1 and A_2, respectively.

To manufacture a self-cleaning surface, not only contact angles higher than 150° are required, but also a low contact angle hysteresis. Both conditions are required to allow water drops roll off on the surface removing dust. This behavior is described by Cassie-Baxter state, according to which the liquid can roll off on the surface leaving a dry base as air is retained inside avoiding the contact [39]. Fig. 7 illustrates differences between receding and advancing contact angles for the coated surfaces after one (Fig. 7 (a)) and three immersions (Fig. 7 (b)). For one immersion, the coatings prepared on A_0 have low hysteresis, showing negligible differences between advancing and receding contact angles, in accordance to Cassie-Baxter state. So, when the surface was tilted (around 5°), the drop rolls off on it. However, the coatings on A_1 and A_2 pretreatments have lower static contact angle and higher hysteresis than the coatings deposited on A_0. Water drops do not roll off. This behavior is described by Wenzel state. Here, the liquid drops wet the tips of pillars and the inside of them, but they do not go into the smaller ones (nanopillars) [39]. The results show that increasing the surface energy of the surface to coat using pretreatments is not the key factor to get superhydropobic properties.

After three immersions, all coatings show static contact angles higher than 150° (Fig. 6) and negligible hysteresis, lower than 3° (Fig. 7 (b)). So, the wetting mechanism after three immersions can be described using Cassie-Baxter state.

The morphology of the coatings was studied by SEM to identify the changes provoked by the coating, leading to superhydrophobicity, as a function of pretreatment and number of immersions. Fig. 8 shows water contact angles and SEM images of superhydrophobic coatings prepared on A_0, A_1 and A_2 (after one immersion).

SEM images show a heterogeneous distribution of SiO_2 aggregates after one immersion, with areas completely free of them for all studied surfaces. Comparing the three surfaces after 1 immersion, the widest coated area is observed for A_0. This explains the highest static contact angles and the lowest hysteresis values measured for the coating deposited on A_0. Water static contact angle images (Fig. 8) confirm the different wetting states (Cassie-Baxter for A_0 and Wenzel for A_1 and A_2), clearly related to the formation of the aggregates. As previously explained, the studied pretreatments (A_0, A_1 and A_2) promote surfaces with different physical and chemical properties. After A_0 pretreatment, the original (as received) passive film is being observed, as A_0 only implies a degreasing. This original passive film is richer in iron than in chromium, in contrast to compositions found after A_1 and A_2, being A_0 the surface with lowest wettability (Fig. 4). Therefore, the development of superhydrophobic coatings seems to be related to the elemental composition of the surface, its wettability condition and/or its nanoroughness.

After this first immersion, the obtained surfaces have very similar wettability conditions, as their surface energy values show (Table 4). Surfaces are scarcely wettable and strongly dispersive, and the polarity obtained with pretreatments has disappeared. The amount of SiO_2 aggregates attached onto the surface undergoes a significant raise with the number of immersions, as it can be observed from SEM images (Fig. 9).

Hence, a superhydrophobic coating (with water contact angle higher than 150°) can be obtained after only 1 immersion, as it occurs for A_0 pretreatment (Fig. 6), although an homogeneous coating is not obtained, as it can be appreciated in SEM images of coated steel (Fig. 8). In order to assure superhydrophobic properties according to Cassie-Baxter state, regardless of pretreatment, increasing amount of SiO_2

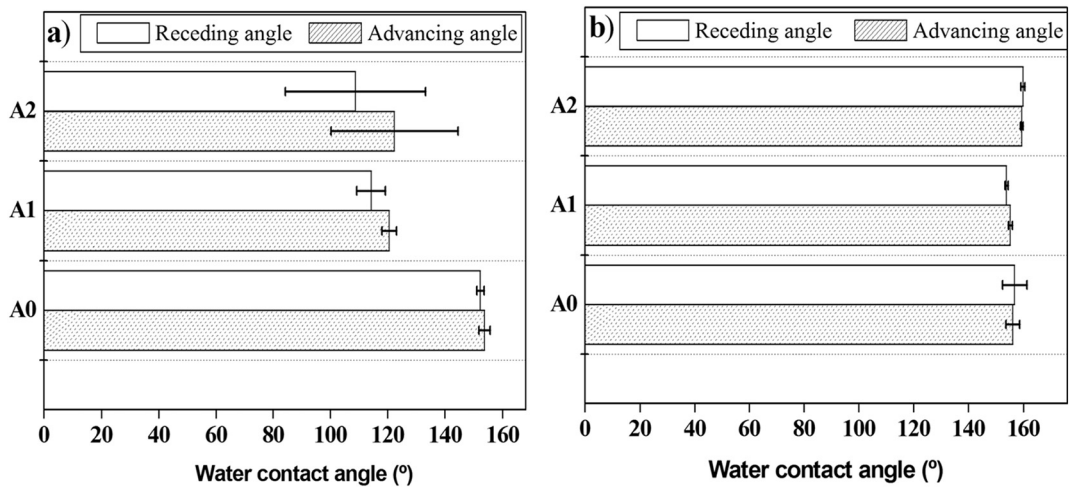

Fig. 7. Advancing and receding water contact angles on coated surfaces for (a) one and (b) three immersions.

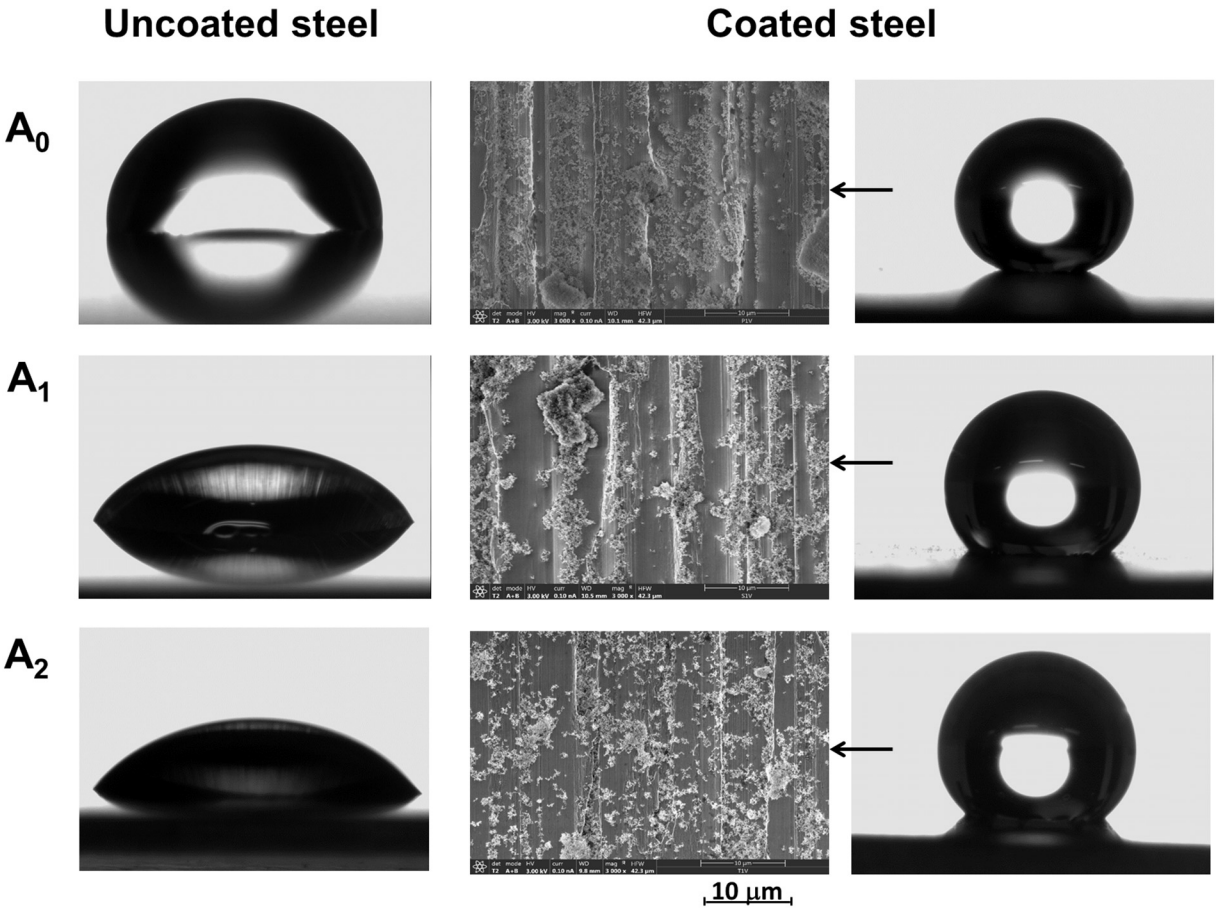

Fig. 8. Water contact angle images of pretreated surfaces (uncoated steel). SEM and water contact angle images of superhydrophobic coatings after 1 immersion (coated steel) for A_0, A_1 and A_2.

Table 4
Surface energy, and its polar and dispersive components, of the coatings after 1 immersion.

	σ_{Total} (mN/m)	σ_{Polar} (mN/m)	$\sigma_{Dispersive}$ (mN/m)
A_0	8.24 ± 1.23	1.21 ± 0.50	7.03 ± 1.12
A_1	6.90 ± 0.95	0.12 ± 0.43	6.77 ± 0.84
A_2	7.49 ± 1.23	0.41 ± 0.43	7.08 ± 1.16

aggregates attached onto the surface using several immersions is required.

To evaluate the robustness of the coatings and their adhesion on steels, a wear test was performed. Results are shown in Fig. 10, for the superhydrophobic coating made on A_0 steel. As it can be observed, water contact angles decrease after abrasion test (both after 1 and 2 cycles) reaching values around 106° (Fig. 10). This surface loses the superhydrophobic properties that previously exhibited. These values of water contact angle are close to those of A_0 steel (Fig. 8). Torun et al. [26] found similar values for a supherhydrophobic glass after a linear abrasion test.

The morphological characteristics of this coating after the abrasion test were analyzed by SEM (Fig. 10 (c)). The network of SiO_2 agglomerates has disappeared, being found a lower amount of nanoparticles on the surface. So, the typical topography of the steel without coating (Fig. 8) is observed again. Silicon amount on the surface, before and after abrasion test, was determined by EDX. Values around 12 ± 3% and 6 ± 2% wt. of silicon were found, respectively. Therefore, this significant reduction of SiO_2 agglomerates on the steel surface can explain the loss of superhydrophobicity.

Similar results are found for A_1 and A_2 coated surfaces, measuring water contact angles lower than 110°. The abrasion performance of these superhydrophobic coatings is not improved with those pretreatments. Therefore, the mechanical robustness of these coatings is very low regardless the pretreatment applied.

4. Conclusions

The chemical pretreatments increase the surface energy (16% for A_1 and 86% for A_2), mainly due to the increase of the polar component (from 8.4 mJ/m^2 for A_0 to 17.2 and 26.3 mJ/m^2 for A_1 and A_2 respectively) and the nanoroughness. It can be explained because these chemical pretreatments remove the most external layers (including surface contamination and iron layer) provoking that the passive layer is strongly Cr-rich, as it was observed by XPS.

Therefore, different tailored surfaces can be obtained in stainless steels using these pretreatments, appearing new surfaces exhibiting different physicochemical characteristics that may influence the formation of superhydrophobic coatings.

After one immersion, static water contact angles higher 150° and hysteresis lower than 2° only are observed for the coatings prepared on A_0, showing a behavior that can be described by Cassie-Baxter state. Wenzel state described the behavior observed on A_1 and A_2, with static water contact angles slightly lower 150° and hysteresis higher than 2°. Pretreated surfaces with low surface energy are important to develop superhydrophobic coatings after 1 immersion in tested silane-based solution. The surface elemental composition is a key factor to reduce surface energy of the steel.

Superhydrophobic properties according to Cassie-Baxter state can

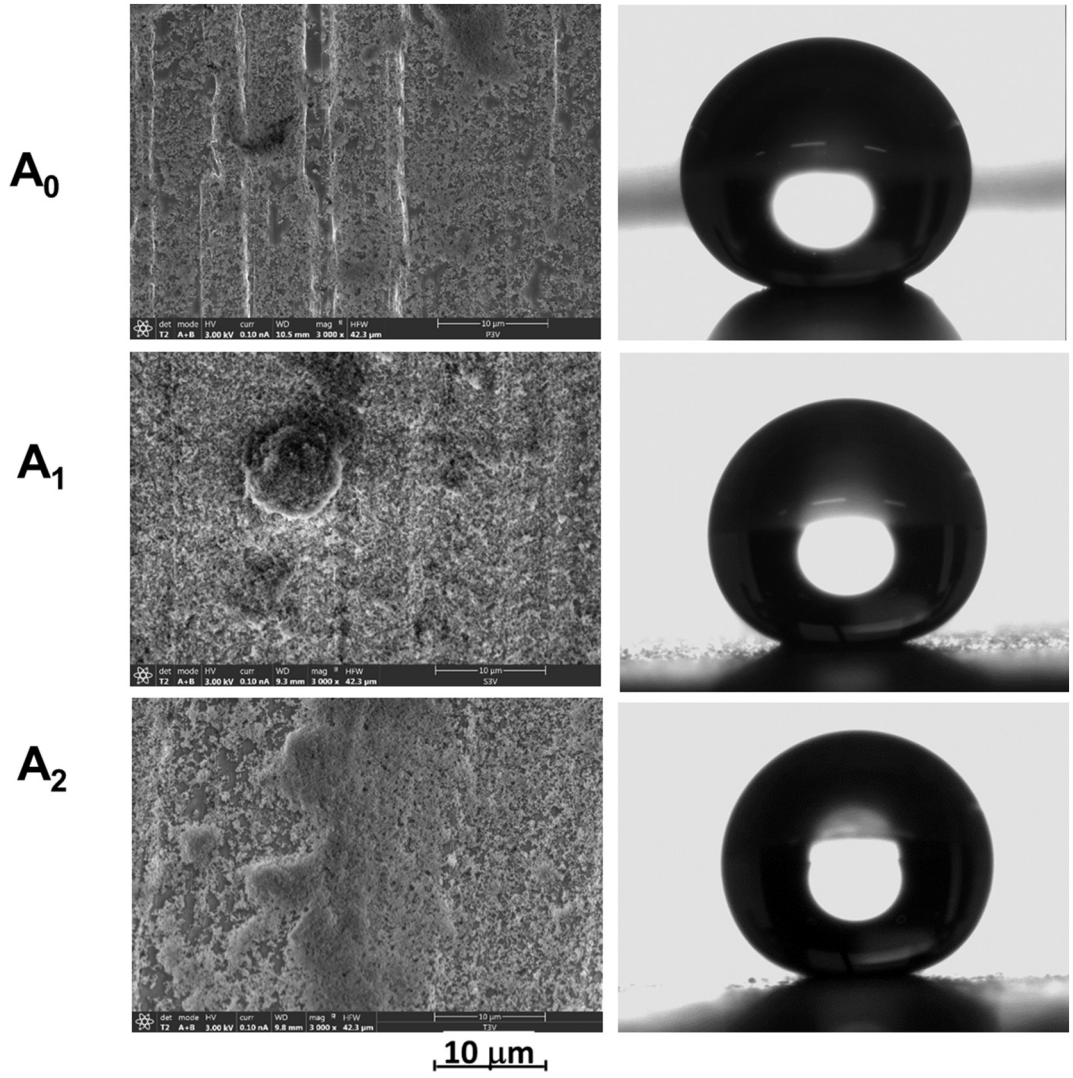

Fig. 9. SEM and water contact angle images of superhydrophobic coatings after 3 immersion on the different pretreated surfaces (A_0, A_1 and A_2).

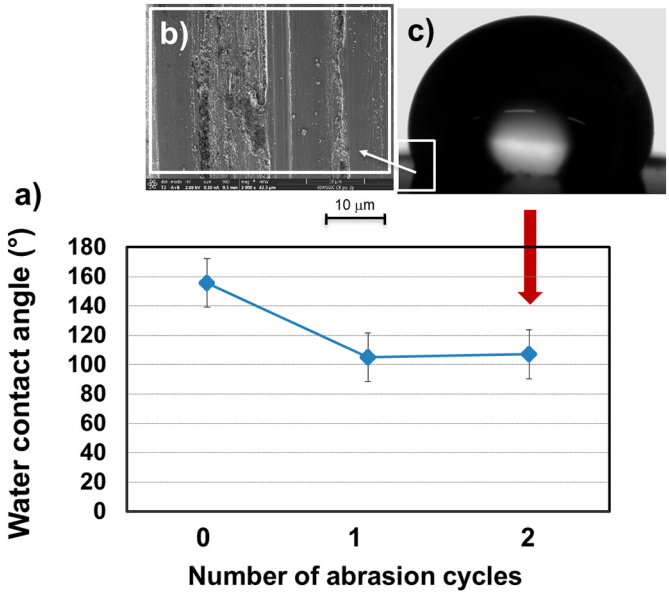

Fig. 10. A_0 coated pretreated steel, 3 immersions coated, (a) Static water contact angle as a function of the number of abrasion cycles, (b) SEM image of wear track, and (c) water contact angle image after 2 abrasion cycles.

be obtained, regardless of pretreatment, increasing amount of SiO_2 aggregates attached onto the surface using several immersions.

The mechanical robustness of these coatings is very low regardless the pretreatment applied.

Acknowledgment

The authors would like to express their gratitude for the financial support of Interreg SUDOE, through KrEaTive Habitat project (Ref. SOE1/P1/E0307).

References

[1] Y. Yan, N. Gao, W. Barthlott, Mimicking natural superhydrophobic surfaces and grasping the wetting process: a review on recent progress in preparing super-hydrophobic surfaces, Adv. Colloid Interf. Sci. 169 (2011) 80–105.
[2] A. Milionis, E. Loth, I. Bayer, Recent advances in the mechanical durability of superhydrophobic materials, Adv. Colloid Interf. Sci. 229 (2016) 57–79.
[3] T. Simovich, A.H. Wu, R.N. Lamb, Hierarchically rough, mechanically durable and superhydrophobic epoxy coatings through rapid evaporation spray method, Thin Solid Films 589 (2015) 472–478.
[4] W. Huang, C. Lin, Robust superhydrophobic transparent coatings fabricated by a low-temperature sol-gel process, Appl. Surf. Sci. 305 (2014) 702–709.
[5] N. Gao, Y.Y. Yan, X.Y. Chen, X.F. Zheng, Superhydrophobic composite films based on THS and nanoparticles, J. Bionic Eng. 7 (2010) S59–S66 Suppl..
[6] N. Gao, Y.Y. Yan, X.Y. Chen, D.J. Mee, Superhydrophobic surfaces with hierarchical structure, Mater. Lett. 65 (2011) 2902–2905.
[7] A. Cholewinski, J. Trinidad, B. McDonald, B. Zhao, Bio-inspired

polydimethylsiloxane-functionalized silica particles-epoxy bilayer as a robust superhydrophobic surface coating, Surf. Coat. Technol. 254 (2014) 230–237.
[8] T.C. Canak, C. Ünsal, I.E. Serhatli, Superhydrophobic fluorinated acrylonitrile coatings via electrospraying, Prog. Org. Coat. 105 (2017) 342–352.
[9] Z. Sun, B. Liu, S. Huang, J. Wu, Q. Zhang, Facile fabrication of superhydrophobic coating based on polysiloxane emulsion, Prog. Org. Coat. 102 ((2017) 131–137.
[10] D. Kumar, X. Wu, Q. Fu, J. Weng, C. Ho, P.D. Kanhere, L. Li, Z. Chen, Development of durable self-cleaning coatings using organic–inorganic hybrid sol–gel method, Appl. Surf. Sci. 344 (2015) 205–212.
[11] S.A. Mahadik, F. Pedraza, R.S. Vhatkar, Silica based superhydrophobic coating for long-term industrial and domestic applications, J. Alloy Compd. 663 (2016) 487–493.
[12] S. Jia, M. Liu, Y. Wu, S. Luo, Y. Qing, H. Chen, Facile and scalable preparation of highly wear-resistance superhydrophobic surface on wood substrates using silica nanoparticles modified by VTES, Appl. Surf. Sci. 386 (2016) 115–124.
[13] N. Yokoi, K. Manabe, M. Tenjimbayashi, S. Shiratori, Optically transparent superhydophobic surfaces with enhanced mechanical abrasion resistance enabled by mesh structure, ACS Appl. Mater. Interface 7 (2015) 4809–4816.
[14] J. Bruzaud, E. Jeanne Tarrade, T. Celia, E. Darmanin, F. Taffin De Givenchy, J. Guittard, M. Herry, M. Bellon-Fontaine Guilbaud, The design of superhydrophobic stainless steel surfaces by controlling nanostructures: a key parameter to reduce the implantation of pathogenic bacteria, Mater. Sci. Eng. C 73 (2017) 40–47.
[15] R.K. Sahoo, A. Das, S.K. Singh, B.K. Mishra, Synthesis of surface modified SiC superhydrophobic coating on stainless steel surface by thermal plasma evaporation method, Surf. Coat. Technol. 307 ((2016) 476–483.
[16] M. Obeidi, E. McCarthy, D. Brabazon, Methodology of laser processing for precise control of surface micro-topology, Surf. Coat. Technol. 307 ((2016) 702–712.
[17] A.A. Serkov, G.A. Shafeev, E.V. Barmina, A. Loufardaki, E. Stratakis, Stainless steel surface wettability control via laser ablation in external electric field, Appl. Phys. A Mater. Sci. Process. 122 (2016) 1067–1072.
[18] M. Martinez-Calderon, A. Rodriguez, A. Dias-Ponte, M.C. Morant-Minana, M. Gomez-Aranzadi, S.M. Olaizola, Femtosecond laser fabrication of highly hydrophobic stainless steel surface with hierarchical structures fabricated by combining ordered microstructures and LIPSS, Appl. Surf. Sci. 374 (2016) 81–89.
[19] Hu Y, H. He, Y. Ma, Preparation of superhydrophobic SiO_2 coating on stainless steel substrate, Key Eng. Mater. 512-515 (2012) 1028–1031.
[20] J. Xu, Y. Liu, W. Du, W. Lei, X. Si, T. Zhou, J. Lin, L. Peng, Superhydrophobic silica antireflective coatings with high transmittance via one-step sol-gel process, Thin Solid Film. 631 (2017) 193–199.
[21] X. Wu, I. Wyman, G. Zhang, J. Lin, Z. Liu, Y. Wang, H. Hu, Preparation of superamphiphobic polymer-based coatings via spray-and dip-coating strategies, Prog. Org. Coat. 90 (2016) 463–471.
[22] Z.Z. Luo, Z.Z. Zhang, W.J. Wang, W.M. Liu, Q.J. Xue, Various curing conditions for controlling PTFE micro/nano-fiber texture of a bionic superhydrophobic coating surface, Mater. Chem. Phys. 119 (2010) 40–47.
[23] F. Velasco, M.A. Martínez, R. Calabrés, A. Bautista, J. Abenojar, Friction of PM ferritic stainless steels at temperatures up to 300 °C, Tribol. Int. 42 (2009) 1199–1205.
[24] A. Bautista, G. Blanco, F. Velasco, M.A. Martínez, Corrosion performance of welded stainless steels reinforcements in simulated pore solutions, Constr. Build. Mater. 21 (2007) 1267–1276.
[25] M. Pantoja, J. Abenojar, M.A. Martinez, Influence of the type of solvent on the development of superhydrophobicity from silane-based solution containing nanoparticles, Appl. Surf. Sci. 397 (2017) 87–94.
[26] I. Torun, M. Serdar Onses, Robust superhydrophobicity on paper: Protection of spray-coated nanoparticles against mechanical wear by the microstructure of paper, Surf. Coat. Technol. 319 (2017) 301–308.
[27] X. Tian, T. Verho, R.H.A. Ras, Moving superhydrophobic surfaces toward real-world applications, Science 352 (2016) 142–143.
[28] C. Donik, A. Kocijan, J.T. Grant, M. Jenko, A. Drenik, B. Pihlar, XPS study of duplex stainless steel oxidized by oxygen atoms, Corros. Sci. 51 (2009) 827–832.
[29] P. Ghods, O.B. Isgor, J.R. Brown, F. Bensebaa, D. Kingston, XPS depth profiling study on the passive oxide film of carbon steel in saturated calcium hydroxide solution and the effect of chloride on the film properties, Appl. Surf. Sci. 257 (2011) 4669–4677.
[30] J.F. Moulder, W.F. Stickle, P.E. Sobol, K.D. Bomben, Handbook of X-Ray Photoelectron Spectroscopy, Physical Electronics Inc, Minnesota, 1992.
[31] A.A. Hermas, XPS analysis of the passive film formed on austenitic stainless steel coated with conductive polymer, Corros. Sci. 50 (2008) 2498–2505.
[32] F. Gaoutier, S. Valette, E. Laborde, P. Lefort, 304L stainless steel oxidation in carbon dioxide: an XPS study, J. Alloy Compd. 509 (2011) 3246–3251.
[33] W. Kuang, X. Wu, E. Han, Influence of dissolved oxygen concentration on the oxide film formed on 304 stainless steel in high temperature water, Corros. Sci. 63 (2012) 259–266.
[34] Y. Hedberg, M. Karlsson, E. Blomberg, I. Odnevall, J. Hedberg, Correlation between surface physicochemical properties and the release of iron from stainless steel AISI 304 in biological media, Colloid Surf. B 122 (2014) 216–222.
[35] A.R. Brooks, C.R. Clayton, K. Doss, Y.C. Lu, On the role of Cr in the passivity of stainless steel, J. Electrochem. Soc. 133 (1986) 2459–2464.
[36] M. Mantel, J.P. Wightman, Influence of the Surface chemistry on the wettability of stainless steel, Surf. Interface Anal. 21 (1994) 595–605.
[37] V. Prysiazhnyi, Atmospheric pressure plasma treatment and following aging effect of chromium surfaces, J. Surf. Eng. Mater. Adv. Technol. 3 (2013) 138–145.
[38] M. Padial-Molina, P. Galindo-Moreno, J. Fernández-Barbero, F. O'Valle, A. Jódar-Reyes, J. Ortega-Vinuesa, P. Ramón-Torregrosa, Role of wettability and nanoroughness on interactions between osteoblast and modified silicon surfaces, Acta Biomater. 7 (2011) 771–778.
[39] W.A. Daoud, Self-Cleaning Materials and Surfaces. A Nanotechnology Approach, John Wiley & Sons, Hong Kong, 2013.